Report

Current Biology

Polarized Dishevelled dissolution and reassembly drives embryonic axis specification in sea star oocytes

Graphical abstract

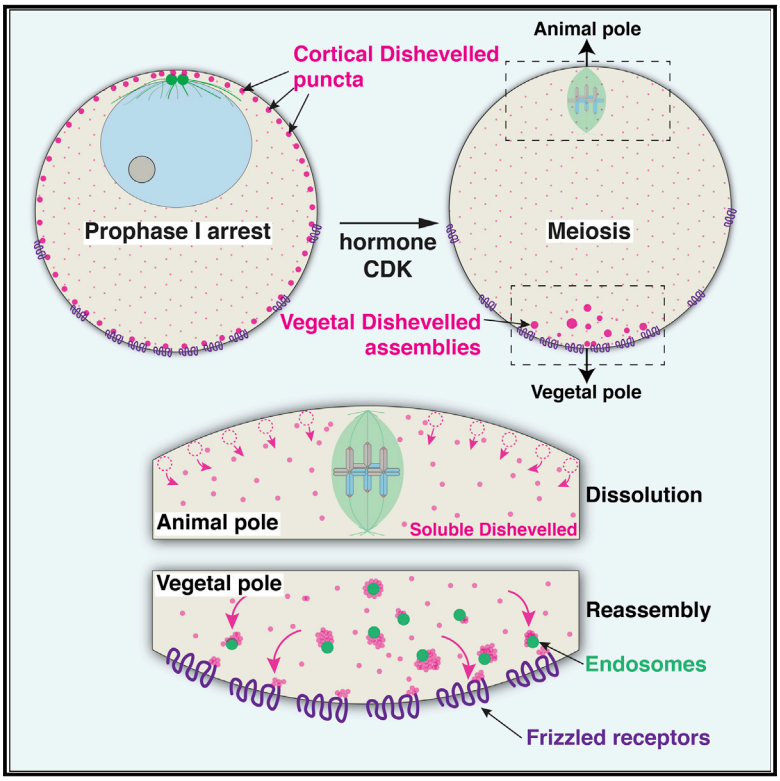

Highlights

- The primary embryonic body axis is maternally specified in sea star oocytes
- Posterior fate specification requires the Wnt pathway effector Dishevelled
- Dishevelled localization polarizes by cell cycle-linked dissolution and reassembly
- Maternal cues and endosome association drive Dishevelled localization

Authors

S. Zachary Swartz, Tzer Han Tan, Margherita Perillo, Nikta Fakhri, Gary M. Wessel, Athula H. Wikramanayake, Iain M. Cheeseman

Correspondence

icheese@wi.mit.edu (I.M.C.), szs@wi.mit.edu (S.Z.S.)

In brief

The primary body axis in diverse species is prefigured within the egg. Using sea star oocytes, Swartz et al. find that the Wnt pathway protein Dishevelled (Dvl) localizes to the vegetal pole to direct body axis specification. Dvl re-localization occurs in meiosis through coupled dissolution and reformation of dynamic molecular assemblies.

Swartz et al., 2021, Current Biology *31*, 5633–5641
December 20, 2021
https://doi.org/10.1016/j.cub.2021.10.022

CellPress

Current Biology

CellPress

Report

Polarized Dishevelled dissolution and reassembly drives embryonic axis specification in sea star oocytes

S. Zachary Swartz,[1,5,*] Tzer Han Tan,[2] Margherita Perillo,[3] Nikta Fakhri,[2] Gary M. Wessel,[3] Athula H. Wikramanayake,[4,5] and Iain M. Cheeseman[1,6,*]

[1]Whitehead Institute for Biomedical Research, Cambridge, MA 02142, USA
[2]Massachusetts Institute of Technology, Department of Physics, Cambridge, MA 02142, USA
[3]MCB Department, Brown University, Providence, RI 02912, USA
[4]Department of Biology, University of Miami, Coral Gables, FL 33134, USA
[5]Embryology Course: Concepts and Techniques in Modern Developmental Biology, Marine Biological Laboratory, Woods Hole, MA 02543, USA
[6]Lead contact
*Correspondence: icheese@wi.mit.edu (I.M.C.), szs@wi.mit.edu (S.Z.S.)
https://doi.org/10.1016/j.cub.2021.10.022

SUMMARY

The organismal body axes that are formed during embryogenesis are intimately linked to intrinsic asymmetries established at the cellular scale in oocytes.[1] However, the mechanisms that generate cellular asymmetries within the oocyte and then transduce that polarity to organismal scale body axes are poorly understood outside of select model organisms. Here, we report an axis-defining event in meiotic oocytes of the sea star *Patiria miniata*. Dishevelled (Dvl) is a cytoplasmic Wnt pathway effector required for axis development in diverse species,[2–4] but the mechanisms governing its function and distribution remain poorly defined. Using time-lapse imaging, we find that Dvl localizes uniformly to puncta throughout the cell cortex in Prophase I-arrested oocytes but becomes enriched at the vegetal pole following meiotic resumption through a dissolution-reassembly mechanism. This process is driven by an initial disassembly phase of Dvl puncta, followed by selective reformation of Dvl assemblies at the vegetal pole. Rather than being driven by Wnt signaling, this localization behavior is coupled to meiotic cell cycle progression and influenced by Lamp1+ endosome association and Frizzled receptors pre-localized within the oocyte cortex. Our results reveal a cell cycle-linked mechanism by which maternal cellular polarity is transduced to the embryo through spatially regulated Dvl dynamics.

RESULTS AND DISCUSSION

Dishevelled is required for specification of the primary body axis in sea star embryos

Developmental determinants of the primary body axis are established maternally within the oocytes of diverse animal species.[5] In many organisms, including echinoderms such as sea stars, the cytologically defined Animal-Vegetal axis of the oocyte correlates with and prefigures the anterior-posterior axis of the embryo (Figure 1A).[5–7] The Wnt/beta-catenin pathway is an important determinant of the primary body axis and provides a link between oocyte asymmetries and embryonic polarity.[8–10] However, the mechanisms by which the Wnt pathway becomes asymmetrically activated within subsets of embryonic cells to direct axis development are poorly defined. Dishevelled (Dvl) is an essential cytoplasmic transducer of Wnt signaling and is localized asymmetrically in diverse organisms, including sea urchin eggs and embryos and in *Xenopus* oocytes following fertilization.[11–14] We sought to define the mechanisms that govern maternal Dvl localization and function, which have been challenging to study in these other systems.

To define the function of Dvl in body axis specification, we used the sea star *Patiria miniata,* which provides a powerful system to study oogenesis, meiosis, and embryogenesis.[15] We found that Dvl depletion using morpholino injection disrupted gastrulation and the expression of known Wnt-beta catenin target genes in the posterior embryo (Figures 1B and 1C),[16] consistent with an essential role for Dvl in primary axis specification and prior dominant-negative studies in sea urchins.[17] We confirmed Dvl depletion by western blotting of 24 h embryos using antibodies raised against *P. miniata* Dvl (Figure S1A). Following 72 h of development, wild-type embryos form a differentiated tripartite gut and mesodermally derived coelomic pouch structures. However, Dvl knockdown embryos failed to form normal endomesodermal structures, indicative of a failure of endomesoderm specification (Figures 1B and 1C). Anterior-posterior patterning is initiated by beta-catenin nuclearization, endomesoderm specification, and the secretion of factors that restrict anterior fate.[16,18,19] These phenotypes are therefore consistent with Dvl acting to specify endomesodermal fates at the posterior pole in the sea star embryo.

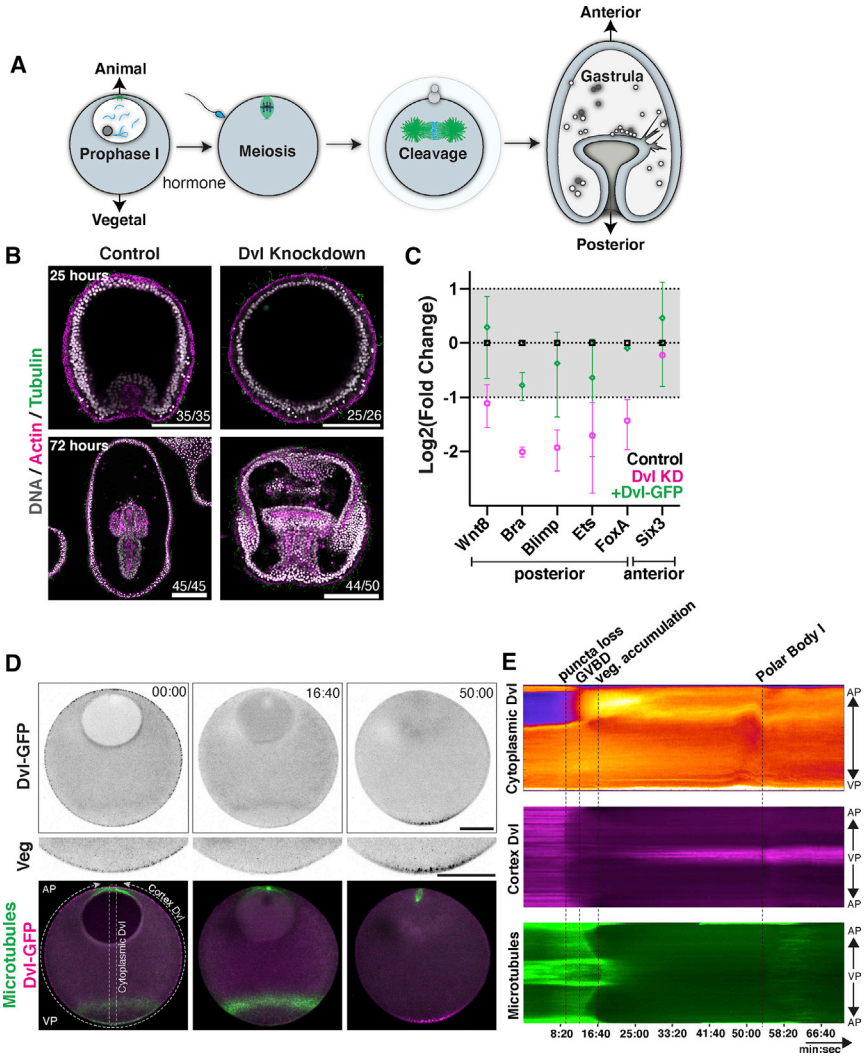

Figure 1. Dishevelled (Dvl) is required for posterior identity and undergoes relocalization in meiosis

(A) Schematic of sea star meiosis and development. The animal-vegetal axis in oocytes, defined by the site of the meiotic divisions, correlates with the anterior-posterior axis in the embryo.

(B) Depletion of Dvl by morpholino injection disrupts primary invagination at the posterior pole (25 h control n = 35, Dvl knockdown n = 26 embryos) and the formation of endomesodermal structures in subsequent embryogenesis (72 h control n = 45, Dvl knockdown n = 50). Scale bars, 50 μm.

(C) Expression of posteriorly expressed cWnt pathway genes is downregulated with Dvl knockdown as measured by qPCR. The anteriorly expressed factor Six3 is unaffected (mean and standard deviation of two biological replicates each performed in technical triplicate).

(D) 4D partial z stacks of live oocyte expressing Dvl-GFP and EMTB-mCherry. Upper images are of Dvl-GFP channel alone in inverted grayscale. In Prophase I arrest (t = 00:00), Dvl localizes to uniformly distributed puncta at the cortex. In addition to the centrosomal microtubule array at the animal pole, EMTB-mCherry revealed a band of microtubule density at the vegetal pole. Following hormonal stimulation, Dvl puncta dissolve (t = 16:40), and then reform at the vegetal pole (t = 50:00). Scale bars, 50 μm.

(E) Kymograph depiction of the oocyte in (D), defined by the white dashed lines in the lower left image. A transverse kymograph of cytoplasmic Dvl, along with circumferential kymographs for cortical Dvl and microtubules are provided. Regions of interest to which the kymographs correspond are outlined in (D).

See also Figure S1 and Video S1.

Dishevelled localization becomes polarized during meiotic cell cycle progression

Given the essential role of Dvl in axis determination, we next sought to define its localization during the oocyte-to-embryo transition by live imaging (Figure 1D; Video S1). In Prophase I-arrested oocytes, Dvl-GFP localized to puncta uniformly throughout the cell cortex, as well as diffusely to the cytoplasm (Figures 1D and 1E). However, following hormonal stimulation, just prior to germinal vesicle breakdown, these Dvl-GFP puncta were lost (Figures 1D and 1E, 16:40). Subsequently, Dvl-GFP assemblies reappeared in the vegetal subcortical cytoplasm as the first meiotic spindle formed. These structures increased in prevalence as the first meiotic division completed (Video S1). Following the completion of meiosis, the first mitotic spindle is oriented perpendicularly with the cleavage plane parallel to the animal-vegetal axis (see also Kitajima et al.[20]). Due to the localization of Dvl to the vegetal pole, this cleavage pattern distributes the vegetal Dvl domain equally to both blastomeres where it remains asymmetrically localized (Figure S1C).

To confirm the behavior observed for ectopically expressed Dvl-GFP, we additionally visualized endogenous Dvl mRNA and protein. Using fluorescent *in situ* hybridization, we detected Dvl mRNA uniformly throughout the oocyte and embryo (Figure S1B). By immunofluorescence, endogenous Dvl protein localized throughout Prophase I-arrested oocytes but formed assemblies that were enriched at the vegetal pole in meiosis (Figure S1C), consistent with our observations of Dvl-GFP. Immunostaining of embryos in which Dvl was knocked down indicated that the antibody selectively recognized Dvl protein (Figure S1D). In summary, Dvl localization becomes polarized in a process coupled temporally to meiotic cell cycle progression, which could serve as a critical event in primary body axis specification during embryogenesis.

Dvl localization to the vegetal pole is correlated temporally with cytological changes during meiotic progression. We therefore considered whether key cell cycle regulators influence Dvl localization. Sea star meiosis occurs largely in the absence of major changes in protein abundance.[21] Consistent with this general protein stability, translational inhibition with emetine did not

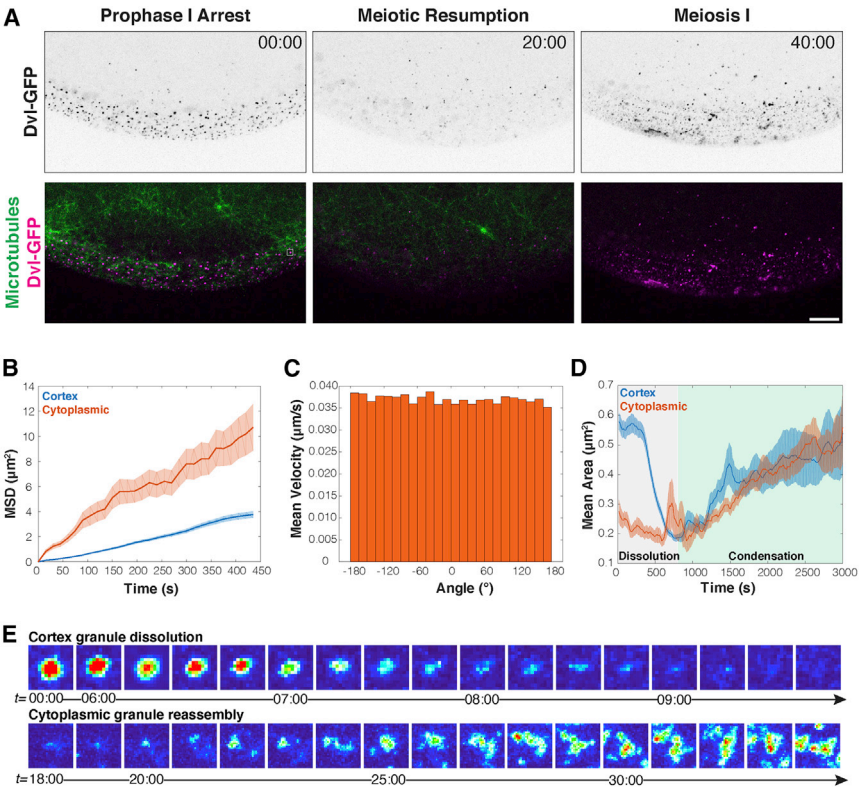

Figure 2. Dishevelled localization by polarized dissolution and condensation

(A) Time-lapse vegetal pole images of oocyte expressing Dvl-GFP and EMTB-mCherry at high magnification (scale bar, 10 μm). Appearance of rows of Dvl-GFP puncta are due to z-step size during rapid acquisition followed by maximal projection. Top images are of the Dvl-GFP channel alone in inverted grayscale.

(B) Mean squared displacement for Dvl assemblies over time, indicating cortex assemblies are less mobile.

(C) Mean velocity of cytoplasmic assemblies across angles relative to the animal-vegetal axis reveals no directionally biased movement.

(D) Area quantification of Dvl assemblies from maximally projected 3D time lapse shown in (A). The images were segmented to separately measure cortex-associated or cytoplasmic assemblies. Area measurements reveal a period of dissolution and condensation for both cytoplasmic and cortex Dvl assemblies. (B, D) Error bars represent the standard error of puncta over time, the sample size of which is provided in Figure S2E.

(E) Magnified views of single Dvl puncta during the dissolution or condensation period. Top row images are 1.5 μm wide, and lower row images are 3.0 μm wide.

See also Figure S2 and Video S2.

affect Dvl vegetal pole relocalization (Figure S2A). In contrast, inhibiting cyclin-dependent kinase (Cdk) activity with flavopiridol to disrupt meiotic progression prevented vegetal Dvl localization (Figure S2A). Cdk and other meiotic kinases are opposed by the protein phosphatases PP1 and PP2A. PP1/PP2A inhibition is sufficient to induce partial meiotic resumption, even in the absence of hormonal stimulation.[21] PP1 and PP2A inhibition using Calyculin A in arrested oocytes was sufficient to induce the dissolution of uniformly distributed Dvl puncta (Figure S2B). However, it did not result in vegetal Dvl localization. Collectively, we propose that the Dvl dissolution and reassembly phases are separable events that require distinct post-translational mechanisms. Dvl reassembly may require the activity of a kinase downstream of hormonal stimulation, possibly including Cdk itself.

Polarized dissolution and reassembly coupled to meiotic progression drives Dvl localization

We next sought to define the mechanisms that underlie Dvl localization to the vegetal pole, including whether this requires cytoplasmic flow or active transport along cytoskeletal elements. We did not observe substantial changes in the bulk cytoplasmic Dvl-GFP concentration along the animal-vegetal (AV) axis when viewed as kymograph over meiotic time (Figure 1E). Furthermore, we did not observe Dvl puncta moving substantial distances across the oocyte, arguing against the presence of directional transport. In addition, pharmacological disruption of microtubule or actin networks did not prevent Dvl vegetal enrichment following hormonal stimulation (Figures S2C and S2D), suggesting that Dvl distribution occurs through alternative mechanisms.

Given the lack of visible transport of Dvl puncta across the oocyte, we instead hypothesized that Dvl enrichment to the vegetal pole is a regionalized process. To analyze this behavior, we specifically imaged the vegetal pole at higher magnification and performed particle tracking analyses. This unbiased analysis revealed two discrete populations of Dvl granules based on proximity to the cell surface (Figure 2A; Video S2)—one in the cytoplasm, and another in close association (<3.25 μm) with the cell surface (Video S2). We therefore tracked these two populations over time separately to assess their differential behaviors (Video S2, middle and bottom panels). Mean squared displacement measurements indicated that the vegetal cortex granules are largely immobile and achieve lower velocities, whereas the cytoplasmic granules traverse greater distances (Figure 2B; Figure S2D). However, on a population level, the movements of the cytoplasmic granules were not directionally biased, based on the mean velocities of all particle trajectories across angles relative to the AV axis (Figure 2C). We therefore conclude that polarized Dvl localization is not a result of directional transport or flow.

Dvl self-assembles into higher order structures via its N-terminal DIX domain and central DEP domain.[22] We therefore hypothesized that biased assembly and disassembly from a uniformly available pool of monomers could favor Dvl puncta assembly at the vegetal pole but disfavor Dvl assembly in the animal region of the oocyte. To test this, we measured the size of Dvl assemblies over time, using the area of maximally projected time-lapse videos as a proxy. In Prophase I-arrested oocytes, the cortex-associated granules were larger and more abundant than the cytoplasmic granules. However, following hormonal stimulation, the size of cortex-associated Dvl puncta decreased rapidly,

displaying behavior characteristic of dissolution (Figures 2D and 2E; FigureS2C). As meiosis progressed, both the cortex and cytoplasmic granules began to reform, reaching a mean area of approximately 0.5 μm^2 (Figures 2D and 2E). Given this strikingly dynamic behavior in response to hormonal signaling, we conclude that Dvl localization is a result of polarized dissolution and reassembly. This process occurs through biochemical signals downstream of meiotic resumption, and is spatially regulated to asymmetrically favor Dvl self-association at the vegetal pole.

Dvl granules are dynamic molecular assemblies

The rapid dissolution and reformation behavior suggests that Dvl incorporates into dynamic molecular assemblies. Indeed, by time-lapse imaging, we identified fusion events among the mobile cytoplasmic Dvl granules suggesting that these assemblies engage in higher-order molecular interactions (Figure 3A; Video S3) . To test the nature of Dvl binding within the larger assemblies, we conducted fluorescent recovery after photobleaching (FRAP) on the cortical Dvl puncta in Prophase I-arrested oocytes and on the immobile puncta at the vegetal cortex after Dvl relocalization (Figures 3B and 3C). We found that Dvl exchanged readily between the puncta and cytoplasmic pool with a halftime for recovery of ~2.5 min for both cortical and vegetal cortex-localized granules. However, although Prophase I assemblies recovered fully (mobile fraction = 1.05+/−0.32 SD), the vegetal cortically localized granules displayed lower recovery (mobile fraction = 0.66+/−0.19 SD) (Figure 3C). These differences may reflect different binding modes for Dvl in these different contexts, such as a distinct vegetal receptor for Dvl in meiosis from that in Prophase I-arrested oocytes. Although these data do not allow us to determine conclusively the physical nature of the phase transition state that Dvl undergoes, based on the dynamic properties measured by FRAP and the ability of assemblies to fuse, we propose that Dvl forms dynamic biomolecular assemblies, which may form by phase-separation or using structured protein-protein interactions.

Dvl assemblies associate with Lamp1-positive endosomes

The molecular interactions and cellular states driving Dvl self-association into punctate structures are not well understood.[22] The distinct Dvl populations within the oocyte display differing properties, which could reflect different binding partners or differing microenvironments. The movement and geometry of cytoplasmic Dvl assemblies suggest that they are influenced by interactions with cellular structures (Figures 2A and 3A;Video S2). To test this, we visualized endomembrane compartments, including putative lysosomes as labeled with Lamp1-3xGFP. We observed a striking association between Dvl-GFP granules and the surface of Lamp1-positive endosomes (Figures 3D and 3F; Video S4). Dvl-associated endosomes were also Rab7 positive, suggesting a subclass of late endosomes or lysosome-related organelles (Figures S3A and S3B). Immunofluorescence further revealed that endogenous Dvl protein assembled into granules that co-localized with Lamp1-positive endosomes (Figures S3C and S3D). This unexpected interaction between Dvl granules and Lamp1-positive endosomes could facilitate nucleation of Dvl assemblies or serve as anchors to retain them at the oocyte's vegetal pole. Based on image segmentation, the relative proportion of Dvl in granules associated with endosomes was low in Prophase I and peaked in meiosis I (Figure 3E), consistent with cell cycle regulation. Furthermore, the association with Dvl assemblies was maintained stably even as the endosomes moved (Figure 3G; Video S4). We hypothesize that Dvl assembly on the surface of these endosomes could provide a reservoir of Dvl protein that stably maintains the vegetal Dvl domain as the cortex is remodeled across the cell cycle. Endocytosis has been found to play an important role in Wnt signaling downstream of Frizzled receptors[23] and may also be necessary here for Dvl localization in oocytes.

We next evaluated which Dvl protein regions mediate interaction with endosomes. Prior work identified residues within the DIX domain that bind actin and lipids *in vitro* and are necessary for Dvl self-association.[4,24,25] These residues were later found to be important for Dvl localization and function in sea urchin embryos.[12,17] We found that mutations in the putative actin and lipid binding domains in sea star Dvl (K47A, and K57A K58A, respectively) were deficient in their ability to localize to uniform puncta in Prophase I-arrested oocytes (Figure S3E). These substitutions may interfere with the ability of Dvl to oligomerize via its DIX domain or to associate with a specific binding partner in Prophase I.[25] However, in contrast with prior work in sea urchins, both mutants were capable of localizing to the vegetal pole following hormonal stimulation, as well as endosome association (Figure S3F).[17] This distinction could represent a species difference or differential localization requirements in meiosis versus embryogenesis.

Pre-localized cues are required for vegetal Dvl assembly

The polarization of Dvl localization occurs in single oocytes denuded of associated somatic cells in open seawater. Because this would preclude Wnt signaling from an adjacent cell, we reasoned that Dvl must be autonomously regulated within the oocyte. We first hypothesized that a gradient of diffusible factors influences Dvl behavior, analogous to MEX-5 regulation of P-granules in *C. elegans* or the CyclinB-Cdk1 activity gradient in sea star oocytes.[26,27] In this model, a repressive signal from the animal pole could prevent Dvl condensation except at the point farthest from its source. Importantly, such a gradient system would be sensitive to changes in oocyte geometry. Therefore, we used microfabricated oval-shaped polydimethylsiloxane (PDMS) chambers to alter oocyte shape by shortening the AV axis (Figure S4A).[28,29] If proximity to the animal pole represses Dvl granule formation, this shape change would cause Dvl to condense at the corners of the oval—the points farthest from the animal pole. Instead, we found that Dvl-GFP localized to the original vegetal pole within the microtubule ring (Figure S4B). This suggests that a cortical cue, rather than an activity gradient, regulates the reassembly of Dvl at the vegetal pole.

We next tested whether the vegetal cortex and adjacent cytoplasm contain pre-established signals that enable Dvl condensation. Using microdissection, we removed the vegetal portion of the oocyte during Prophase I arrest prior to Dvl polarization (Figure 4A). As a control, we removed an equivalent amount of the lateral side of the oocyte cortex and cytoplasm. In vegetally cut oocytes, Dvl-GFP assemblies failed to reform at the vegetal pole during meiosis (Figures 4A and 4B). Immunofluorescence of

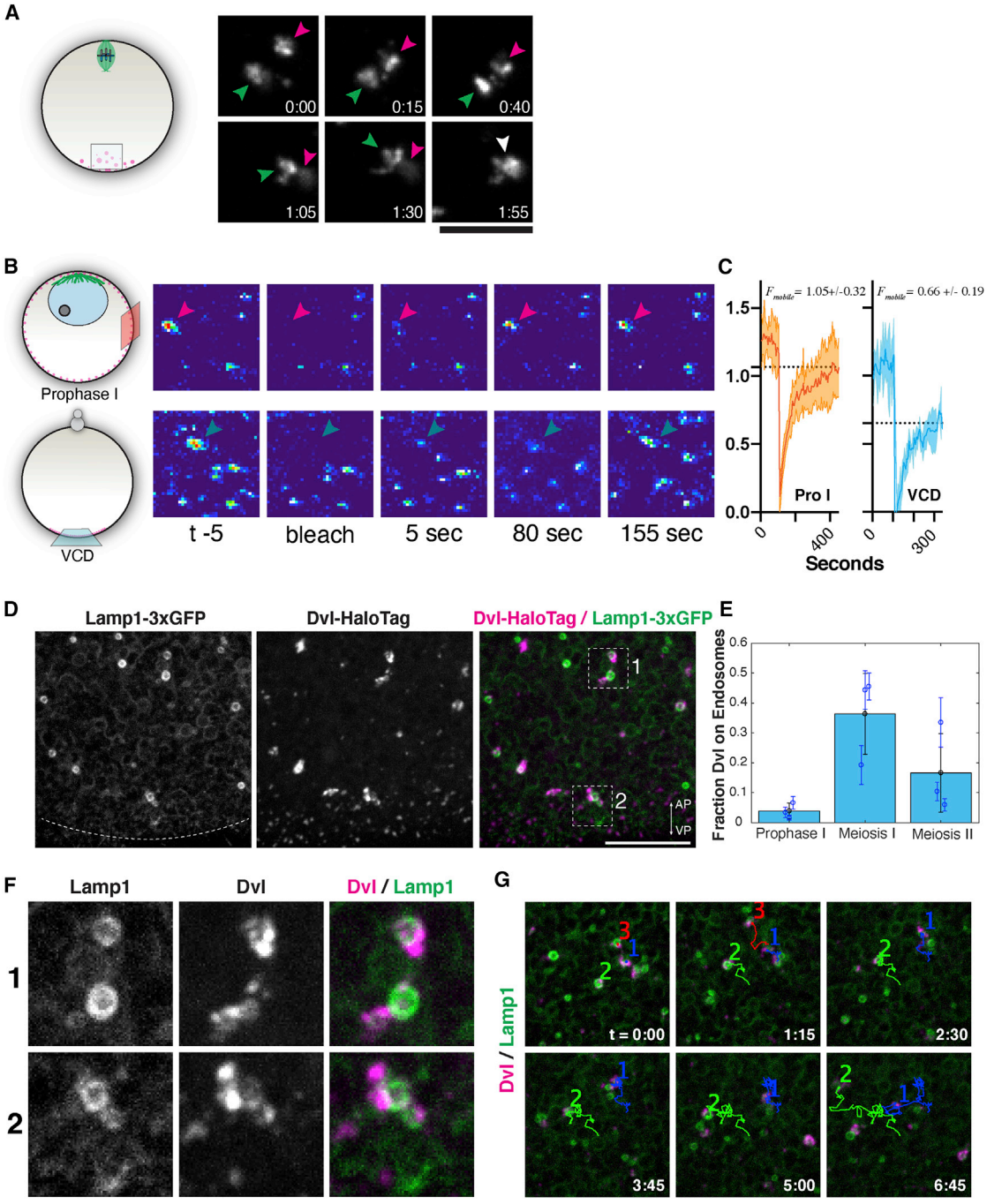

Figure 3. Dishevelled forms dynamic molecular assemblies and associates with cytoplasmic organelles

(A) Time-lapse video stills of a cytoplasmic Dvl assembly (in area schematized to the right) undergoing fusion. Arrowheads indicate the two separate assemblies. Scale bar, 8 μm.

(B) FRAP analysis of uniform cortex puncta in Prophase I, or vegetal cortical domain (VCD) puncta in meiosis. Stills from example FRAP experiments are provided (images are 7.89 μm wide).

(C) FRAP quantification of Prophase I or VCD granules (shaded area represents mean and standard deviation, Pro I n = 6 oocytes, mean of 3 puncta each, VCD n = 4 oocytes, mean of 3 puncta each).

(D) Vegetal pole image of a live oocyte expressing Lamp1-3xGFP and Dvl-HaloTag showing cytoplasmic Dvl assemblies are associated with endosomes. Scale bar, 10 μm.

(E) Fraction of Dvl assemblies that co-localize with Lamp1-positive endosomes in Prophase I, Meiosis I, and Meiosis II. Black circle is the mean value over N = 3 oocytes while blue circle is the number from individual oocyte. Error bars represent the standard deviation over 10 min time lapse videos.

(legend continued on next page)

vegetally cut oocytes for endogenous Dvl yielded similar results (Figure S4C). Reciprocally, isolated vegetal oocyte fragments displayed autonomous Dvl-GFP assembly in response to hormonal stimulation, suggesting that the vegetal region is capable of directing Dvl reassembly in the absence of other cellular structures or signals (Figure 4B). Vegetally ablated oocytes matured and fertilized normally but produced embryos that failed to gastrulate, consistent with a primary axis defect (Figure S4D, see also Kuraishi et al.[30]). Thus, a cue established at the vegetal pole prior to meiotic resumption is essential for the subsequent local Dvl reassembly, which in turn is necessary for gastrulation during embryogenesis.

Maternally expressed Frizzled 1 is required for Dvl localization

Based on our microdissection experiments, we reasoned that a pre-localized membrane-associated factor drives vegetal Dvl reassembly. Dvl can be recruited to the membrane through interactions with Frizzled transmembrane receptors, which detect Wnt signals. Analysis of a sea star ovary transcriptome revealed the expression of Frizzled 1 (Fzd1).[31] By fluorescent *in situ* analysis, we found that Fzd1 mRNA is present in small primordial oocytes and large, full-grown oocytes (Figure S4E). Strikingly, ectopically expressed Fzd1-GFP localized to punctate structures that were enriched toward the vegetal pole in prophase I-arrested oocytes (Figure 4C; Figure S4F). Fzd1 also localized to larger cytoplasmic compartments, possibly corresponding to the Golgi apparatus, in a gradient that was strongest at the vegetal pole, suggesting polarized trafficking of Fzd1 to the vegetal membrane. Consistent with a role in Dvl localization, we observed substantial colocalization between endogenous Dvl assemblies and Fzd1-GFP puncta at the vegetal pole (Figure 4D).

We next tested whether Fzd1 is required for Dvl localization by maternal knockdown. In contrast to controls, Fzd1-depleted embryos displayed significantly reduced punctate Dvl localization to the vegetal cortex (Figures 4D and 4E). Dvl localization was rescued and further increased by expressing knockdown-insensitive Fzd1-GFP (Figures 4D and 4E). Collectively, these results indicate that Fzd1 is localized maternally to the vegetal pole and is essential for Dvl localization to the vegetal cortex. However, although Fzd1-GFP is vegetally enriched, it is present throughout the oocyte, suggesting other mechanisms are additionally required to restrict Dvl to the vegetal pole.

A conserved paradigm for primary body axis specification in animals

A fundamental problem in development is the generation of asymmetries along body axes to pattern a multi-functionalized body plan. Comparative studies point to asymmetric activation of the Wnt pathway as a deeply conserved determinant of the primary body axis in both cnidarians and bilaterian animals.[8,10] Here, we identified a symmetry-determining event involving the Wnt pathway effector Dvl. In contrast to other polarization events influenced by sperm entry, such as in *C. elegans*, the sea star body axis is specified entirely by maternal control. We find that Dvl undergoes a cycle of polarized dissolution and reassembly to distribute asymmetrically to the vegetal pole. This redistribution is essential for primary axis specification and is regulated cell-autonomously during meiotic progression and by cues including the receptor Fzd1, which are prelocalized to the vegetal pole.

Dvl has been noted to form large "puncta" or "granules" in several animal models, as well as by overexpression experiments in mammalian cell culture, but the physiological relevance and mechanisms by which these granules form has been debated.[32,33] Here, we define a paradigm by which Dvl granules form at endogenous levels. An important future direction will be to determine the biophysical mechanisms underlying this dissolution-reassembly process. The ability of Dvl to self-associate through multivalent interactions to form dynamic assemblies could suggest a phase separation-based mechanism.[22,34] The switch-like response of cortical Dvl dissolution dynamics in response to hormonal reception (<5 min, Figures 1E and 2C) could result from a rapidly propagating signaling wave that lowers the condensation point of Dvl puncta across the cortex. In contrast, the gradual reassembly process (>30 min, Figures 1E and 2C) suggests a nucleation-and-growth process by condensation that is seeded by endosomes and Fzd1 in a diffusion-limited manner. Alternatively, Dvl granules could instead form through canonical, structured interactions.

Prior work has identified potential associations between Dvl and endomembrane compartments, including putative vesicle-related organelles in *Xenopus* oocytes, although the physiological significance of these interactions remains unclear.[2,4,13,24] Similarly, interactions with endoplasmic reticulum regulate the biogenesis and fission of membraneless organelles including p-bodies and stress granules,[35] suggesting that endomembrane associations may broadly regulate protein assemblies such as Dvl granules. In sea star meiosis, we identified stable associations between Dvl and endosomes (Figures 3D–3G), which could provide a local reservoir of Dvl protein to support a stable posterior-specifying signaling domain through the meiotic and embryonic mitotic divisions. Putative lipid-binding residues within the Dvl DIX domain are dispensable for this association and instead suggest that it may occur through a specific binding partner, such as Frizzled receptors internalized by endocytosis.[4,12,17,23] Given the broad diversity of organisms in which Dvl granule formation has been observed, Dvl and its capacity for spatially regulated self-assembly may occupy a critical node in the evolution of the Metazoan body plan.

STAR★METHODS

Detailed methods are provided in the online version of this paper and include the following:

- KEY RESOURCES TABLE

(F) Zoom views of insets indicated in (D). Images are 4.88 μm wide.
(G) Still images of individual Dvl-endosome complexes tracked over time. Images are 16.93 μm wide.
See also Figure S3 and Videos S3 and S4.

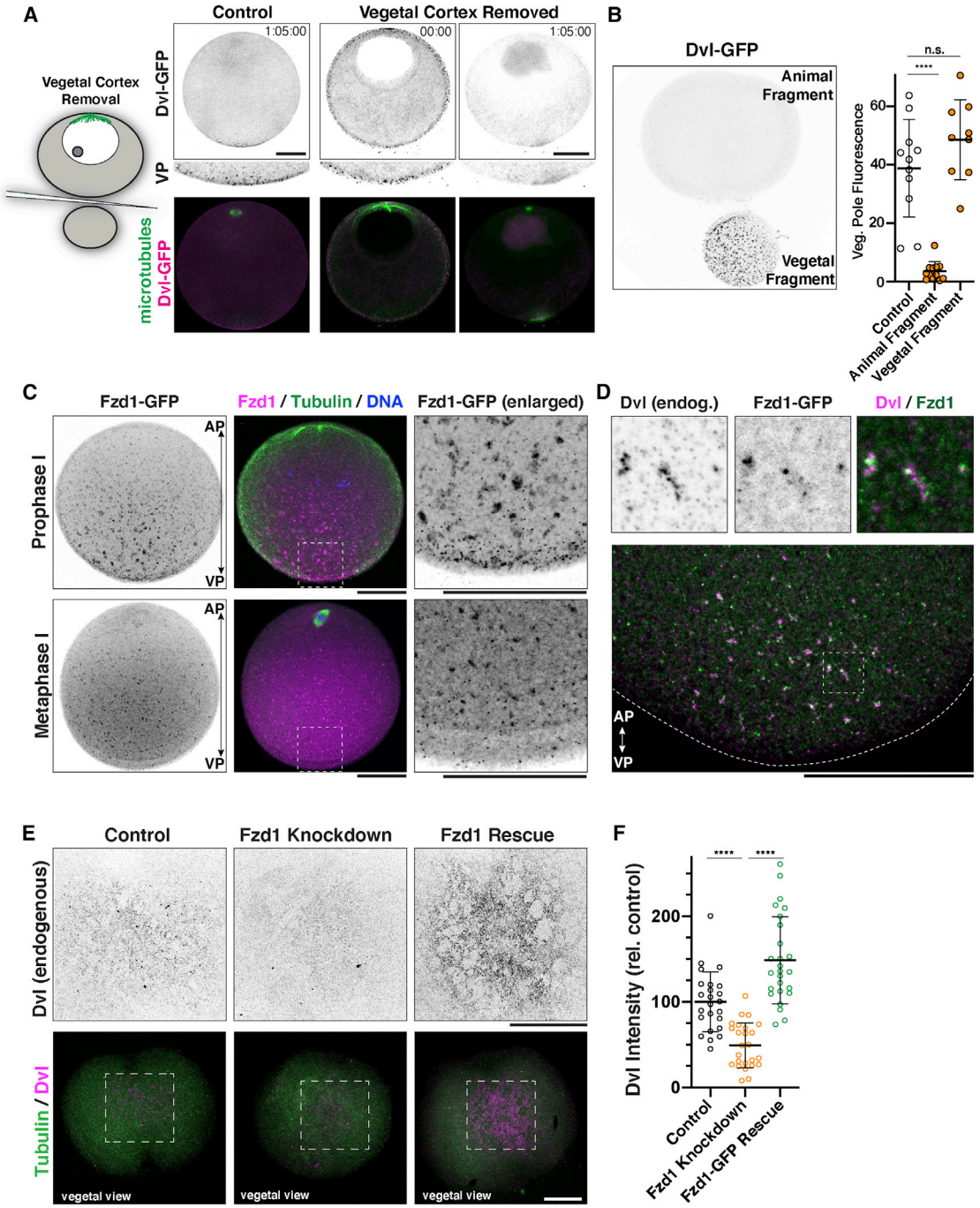

Figure 4. Localization mechanisms driving Dishevelled behavior

(A) Live oocytes expressing Dvl-GFP and EMTB-mCherry from which the vegetal pole was removed by microdissection as described by schematic to the right. As a control, the side of the oocyte was removed. Upper images are Dvl-GFP alone in inverted grayscale. Scale bars, 50 μm.

(B) Dvl-GFP Pixel intensity quantification of vegetal regions of control or vegetally cut animal fragments, and isolated vegetal fragments (error bars represent the mean and standard deviation, control n = 11, animal fragment n = 12, vegetal fragment n = 9 oocytes, ****p < 0.0001 Mann Whitney test).

(C) Expression of GFP-tagged Frizzled 1(Fzd1) in Prophase I arrested and metaphase I oocytes, displayed as partial z stacks. Fzd1 localization is enriched toward the vegetal cortex. Left panels are magnified views of insets.

(D) Immunofluorescence images of endogenous Dvl in colocalization with Fzd1-GFP. Upper images are magnified views of inset indicated below. Scale bars, 50 μm.

(E) Immunofluorescence images of endogenous Dvl in two-cell embryos following control injection, Fzd1 morpholino, or morpholino combined with Fzd1-GFP overexpression. Scale bars, 50 μm.

(F) Relative pixel intensity quantification of vegetal cortex Dvl signal (error bars represent the mean and standard deviation, control n = 24, Fzd1 knockdown n = 25, Fzd1 overexpression n = 26 oocytes, ****p < 0.0001Mann-Whitney Test).

See also Figure S4.

SUPPLEMENTAL INFORMATION

Supplemental information can be found online at https://doi.org/10.1016/j.cub.2021.10.022.

ACKNOWLEDGMENTS

We thank the Marine Biological Laboratory and the students, faculty, and staff of the Embryology Course, where the pilot experiments for this work began. We thank Gene-Tools for donating the PmDvl morpholino to the course. We thank Hannah Rosenblatt for suggesting an examination of lysosomes. We thank Peter Lenart, Brad Shuster, Peter Reddien, and members of the Cheeseman laboratory for helpful discussions. We thank Veronica Hinman and her laboratory for sharing *in situ* probes. This research was supported by grants from the NIH to S.Z.S. (K99HD099315), I.M.C. (R35GM126930), and the MBL Embryology Course (R25HD094666), and grants to I.M.C. and N.F. from the Gordon and Betty Moore Foundation., United States

AUTHOR CONTRIBUTIONS

Conceptualization, S.Z.S., A.H.W., and I.M.C.; methodology, S.Z.S., T.H.T., and M.P.; aalidation, S.Z.S., T.H.T., and M.P.; formal analysis, S.Z.S. and T.H.T.; investigation, S.Z.S. and M.P.; writing – original draft, S.Z.S. and I.M.C.; writing – review & editing, S.Z.S., T.H.T., M.P., G.M.W., A.H.W., and I.M.C.; visualization, S.Z.S., T.H.T., and M.P.; supervision, N.F., G.M.W., A.H.W., and I.M.C.; funding acquisition, S.Z.S. and I.M.C.

DECLARATION OF INTERESTS

I.M.C. is a member of the Editorial Advisory Board for *Current Biology*.

Received: May 13, 2021
Revised: August 20, 2021
Accepted: October 8, 2021
Published: November 4, 2021

REFERENCES

1. St Johnston, D., and Ahringer, J. (2010). Cell polarity in eggs and epithelia: parallels and diversity. Cell *141*, 757–774.
2. Schwarz-Romond, T., Merrifield, C., Nichols, B.J., and Bienz, M. (2005). The Wnt signalling effector Dishevelled forms dynamic protein assemblies rather than stable associations with cytoplasmic vesicles. J. Cell Sci. *118*, 5269–5277.
3. Schaefer, K.N., and Peifer, M. (2019). Wnt/Beta-Catenin Signaling Regulation and a Role for Biomolecular Condensates. Dev. Cell *48*, 429–444.
4. Capelluto, D.G., Kutateladze, T.G., Habas, R., Finkielstein, C.V., He, X., and Overduin, M. (2002). The DIX domain targets dishevelled to actin stress fibres and vesicular membranes. Nature *419*, 726–729.
5. Wikramanayake, A.H. (2013). Heads or Tails? Karl Ernst von Baer, Robert Remak, and characterization of the primary axis in animal eggs. Mol. Reprod. Dev. *80*, i.
6. Martindale, M.Q. (2005). The evolution of metazoan axial properties. Nat. Rev. Genet. *6*, 917–927.
7. Kominami, T. (1983). Establishment of embryonic axes in larvae of the starfish, Asterina pectinifera. J. Embryol. Exp. Morphol. *75*, 87–100.
8. Martindale, M.Q., and Hejnol, A. (2009). A developmental perspective: changes in the position of the blastopore during bilaterian evolution. Dev. Cell *17*, 162–174.
9. Wikramanayake, A.H., Hong, M., Lee, P.N., Pang, K., Byrum, C.A., Bince, J.M., Xu, R., and Martindale, M.Q. (2003). An ancient role for nuclear beta-catenin in the evolution of axial polarity and germ layer segregation. Nature *426*, 446–450.
10. Petersen, C.P., and Reddien, P.W. (2009). Wnt signaling and the polarity of the primary body axis. Cell *139*, 1056–1068.
11. Peng, C.J., and Wikramanayake, A.H. (2013). Differential regulation of disheveled in a novel vegetal cortical domain in sea urchin eggs and embryos: implications for the localized activation of canonical Wnt signaling. PLoS ONE *8*, e80693.
12. Leonard, J.D., and Ettensohn, C.A. (2007). Analysis of dishevelled localization and function in the early sea urchin embryo. Dev. Biol. *306*, 50–65.
13. Miller, J.R., Rowning, B.A., Larabell, C.A., Yang-Snyder, J.A., Bates, R.L., and Moon, R.T. (1999). Establishment of the dorsal-ventral axis in Xenopus embryos coincides with the dorsal enrichment of dishevelled that is dependent on cortical rotation. J. Cell Biol. *146*, 427–437.
14. Lee, P.N., Kumburegama, S., Marlow, H.Q., Martindale, M.Q., and Wikramanayake, A.H. (2007). Asymmetric developmental potential along the animal-vegetal axis in the anthozoan cnidarian, Nematostella vectensis, is mediated by Dishevelled. Dev. Biol. *310*, 169–186.
15. Kishimoto, T. (2018). MPF-based meiotic cell cycle control: Half a century of lessons from starfish oocytes. Proc. Jpn. Acad., Ser. B, Phys. Biol. Sci. *94*, 180–203.
16. McCauley, B.S., Akyar, E., Saad, H.R., and Hinman, V.F. (2015). Dose-dependent nuclear β-catenin response segregates endomesoderm along the sea star primary axis. Development *142*, 207–217.
17. Weitzel, H.E., Illies, M.R., Byrum, C.A., Xu, R., Wikramanayake, A.H., and Ettensohn, C.A. (2004). Differential stability of beta-catenin along the animal-vegetal axis of the sea urchin embryo mediated by dishevelled. Development *131*, 2947–2956.
18. Wikramanayake, A.H., Huang, L., and Klein, W.H. (1998). beta-Catenin is essential for patterning the maternally specified animal-vegetal axis in the sea urchin embryo. Proc. Natl. Acad. Sci. USA *95*, 9343–9348.
19. Range, R.C., Angerer, R.C., and Angerer, L.M. (2013). Integration of canonical and noncanonical Wnt signaling pathways patterns the neuroectoderm along the anterior-posterior axis of sea urchin embryos. PLoS Biol. *11*, e1001467.
20. Kitajima, A., and Hamaguchi, Y. (2005). Determination of first cleavage plane: the relationships between the orientation of the mitotic apparatus for first cleavage and the position of meiotic division-related structures in starfish eggs. Dev. Biol. *280*, 48–58.
21. Swartz, S.Z., Nguyen, H.T., McEwan, B.C., Adamo, M.E., Cheeseman, I.M., and Kettenbach, A.N. (2021). Selective dephosphorylation by PP2A-B55 directs the meiosis I-meiosis II transition in oocytes. eLife *10*, e70588.
22. Bienz, M. (2020). Head-to-Tail Polymerization in the Assembly of Biomolecular Condensates. Cell *182*, 799–811.
23. Brunt, L., and Scholpp, S. (2018). The function of endocytosis in Wnt signaling. Cell. Mol. Life Sci. *75*, 785–795.
24. Capelluto, D.G., and Overduin, M. (2005). Secondary structure, 1H, 13C and 15N resonance assignments and molecular interactions of the dishevelled DIX domain. J. Biochem. Mol. Biol. *38*, 243–247.
25. Schwarz-Romond, T., Fiedler, M., Shibata, N., Butler, P.J., Kikuchi, A., Higuchi, Y., and Bienz, M. (2007). The DIX domain of Dishevelled confers

Wnt signaling by dynamic polymerization. Nat. Struct. Mol. Biol. *14*, 484–492.

26. Brangwynne, C.P., Eckmann, C.R., Courson, D.S., Rybarska, A., Hoege, C., Gharakhani, J., Jülicher, F., and Hyman, A.A. (2009). Germline P granules are liquid droplets that localize by controlled dissolution/condensation. Science *324*, 1729–1732.
27. Bischof, J., Brand, C.A., Somogyi, K., Májer, I., Thome, S., Mori, M., Schwarz, U.S., and Lénárt, P. (2017). A cdk1 gradient guides surface contraction waves in oocytes. Nat. Commun. *8*, 849.
28. Minc, N., Burgess, D., and Chang, F. (2011). Influence of cell geometry on division-plane positioning. Cell *144*, 414–426.
29. Wigbers, M.C., Tan, T.H., Brauns, F., Liu, J., Swartz, S.Z., Frey, E., and Fakhri, N. (2021). A hierarchy of protein patterns robustly decodes cell shape information. Nat. Phys. *17*, 578–584.
30. Kuraishi, R., and Osanai, K. (1994). Contribution of Maternal Factors and Cellular Interaction to Determination of Archenteron in the Starfish Embryo. Development *120*, 2619–2628.
31. Reich, A., Dunn, C., Akasaka, K., and Wessel, G. (2015). Phylogenomic analyses of Echinodermata support the sister groups of Asterozoa and Echinozoa. PLoS ONE *10*, e0119627.
32. Ma, W., Chen, M., Kang, H., Steinhart, Z., Angers, S., He, X., and Kirschner, M.W. (2020). Single-molecule dynamics of Dishevelled at the plasma membrane and Wnt pathway activation. Proc. Natl. Acad. Sci. USA *117*, 16690–16701.
33. Kan, W., Enos, M.D., Korkmazhan, E., Muennich, S., Chen, D.H., Gammons, M.V., Vasishtha, M., Bienz, M., Dunn, A.R., Skiniotis, G., and Weis, W.I. (2020). Limited dishevelled/Axin oligomerization determines efficiency of Wnt/β-catenin signal transduction. eLife *9*, e55015.
34. Gammons, M.V., Renko, M., Johnson, C.M., Rutherford, T.J., and Bienz, M. (2016). Wnt Signalosome Assembly by DEP Domain Swapping of Dishevelled. Mol. Cell *64*, 92–104.
35. Lee, J.E., Cathey, P.I., Wu, H., Parker, R., and Voeltz, G.K. (2020). Endoplasmic reticulum contact sites regulate the dynamics of membraneless organelles. Science *367*, eaay7108.
36. Miller, A.L., and Bement, W.M. (2009). Regulation of cytokinesis by Rho GTPase flux. Nat. Cell Biol. *11*, 71–77.
37. Schindelin, J., Arganda-Carreras, I., Frise, E., Kaynig, V., Longair, M., Pietzsch, T., Preibisch, S., Rueden, C., Saalfeld, S., Schmid, B., et al. (2012). Fiji: an open-source platform for biological-image analysis. Nat. Methods *9*, 676–682.
38. Swartz, S.Z., McKay, L.S., Su, K.-C., Bury, L., Padeganeh, A., Maddox, P.S., Knouse, K.A., and Cheeseman, I.M. (2019). Quiescent Cells Actively Replenish CENP-A Nucleosomes to Maintain Centromere Identity and Proliferative Potential. Dev. Cell *51*, 35–48.
39. Cary, G.A., Cameron, R.A., and Hinman, V.F. (2018). EchinoBase: Tools for Echinoderm Genome Analyses. Methods Mol. Biol. *1757*, 349–369.
40. Gökirmak, T., Campanale, J.P., Shipp, L.E., Moy, G.W., Tao, H., and Hamdoun, A. (2012). Localization and substrate selectivity of sea urchin multidrug (MDR) efflux transporters. J. Biol. Chem. *287*, 43876–43883.
41. von Dassow, G., Verbrugghe, K.J.C., Miller, A.L., Sider, J.R., and Bement, W.M. (2009). Action at a distance during cytokinesis. J. Cell Biol. *187*, 831–845.
42. Perillo, M., Paganos, P., Spurrell, M., Arnone, M.I., and Wessel, G.M. (2021). Methodology for Whole Mount and Fluorescent RNA In Situ Hybridization in Echinoderms: Single, Double, and Beyond. Methods Mol. Biol. *2219*, 195–216.

STAR★METHODS

KEY RESOURCES TABLE

REAGENT or RESOURCE	SOURCE	IDENTIFIER
Antibodies		
Mouse anti-tubulin (DM1a) unconjugated	Sigma-Aldrich	Cat# T9026; RRID: AB_477593
Rabbit anti-starfish Dvl (1:2000 IF, 1:5000 IB)	This study	N/A
Anti-digoxigenin-peroxidase antibody	Roche	Cat# 11207733910; RRID: AB_514499
GFP Booster ATTO488 antibody	ChromoTek	Cat# gba488-100; RRID: AB_2631386
Chemicals, peptides, and recombinant proteins		
Janelia Fluor 646 HaloTag Ligand	Promega	Cat# GA1120
1-Methyladenine	Acros Organics	Cat# AC201310250
Calyculin A	Santa Cruz Biotechnology	Cat# SC-24000A
Emetine	Sigma Aldrich	Cat# E2375-500MG
Flavopiridol (L86-8275)	Selleckchem	Cat# S1230
Trimethoprim	Santa Cruz Biotechnology	Cat# sc-203302
Sulfamethoxazole	Santa Cruz Biotechnology	Cat# sc-208405
digoxigenin-11-UTP	Sigma Aldrich	Cat# 11277073910
Critical commercial assays		
mMessage mMachine Sp6 Transcription Kit	Thermo Fisher	Cat# AM1340
Poly(A) Tailing Kit	Thermo Fisher	Cat# AM1350
TSA Plus Kit	Perkin-Elmer	Cat# NEL752001KT
Deposited Data		
Raw western blot images and microscopy quantification values	Mendeley Data	https://doi.org/10.17632/z42m3kkvt4.1
Experimental models: Organisms/strains		
Patiria miniata	South-Coast Bio LLC	N/A
Oligonucleotides		
Standard Control Morpholino 5′–CCTCTTACCTCAGTTACAATTTATA–3′	Gene-Tools	N/A
Dishevelled Morpholino 5′—ATGATTTTTGTCTCTTCCATGTTGG—3′	Gene-Tools	N/A
Fzd1 Morpholino 5′—GCTTGACTGAGGATGAAATTTAG—3′	Gene-Tools	N/A
Ubiquitin qPCR primers F: 5′—TTCGGTGAAAGCCAAGATTC—3′ R: 5′—CCCACCTCTCATGGCTAGAA—3′	[16]	N/A
Wnt8 qPCR primers F: 5′—GGGCAGAAACCCAGAACGAC—3′ R: 5′—TACAGCTCCGTGCTTCCCAC—3′	[16]	N/A
Bra qPCR primers F: 5′—CGAGATGATCGTCACCAAGA—3′ R: 5′—GGGGTGAAGTCCAGAAGGAT—3′	[16]	N/A
Blimp1 qPCR primers F: 5′—CCAAACACGACGAAGCACTA—3′ R: 5′—GGCGTTGAGGACAGGTTTAG—3′	[16]	N/A
Ets1/2 qPCR primers F: 5′—ATGCCTGTCTACGCGAGAGT—3′ R: 5′—TCCAGGCTGAACTCCTTGAT—3′	[16]	N/A
FoxA qPCR primers F: 5′—TGGCGCATATAATCCTCACC—3′ R: 5′—GTCTCTCAGTGGCGCAAGAT—3′	[16]	N/A

(*Continued on next page*)

Continued

REAGENT or RESOURCE	SOURCE	IDENTIFIER
Six3 qPCR primers F: 5′—GTGAGACGTTGGAGGAGAGC—3′ R: 5′—TGTGGTTTTCCAGGATGTGA—3′	[16]	N/A
Recombinant DNA		
Dvl-GFP, pCS2+8	This study	pZS217
Dvl-HaloTag, pCS2+8	This study	pZS181
Dvl^{K47A} –GFP, pCS2+8	This study	pZS220
$Dvl^{K57A,K58A}$ –GFP, pCS2+8	This study	pZS221
Lamp1-3xGFP, pCS2+	This study	pZS222
Lamp1-mCherry, pCS2+8	This study	pSZ212
mCherry-Rab7, pCS2+8	This study	pZS218
Frizzled 1 – GFP, pCS2+8	This study	pZS202
GST-Dvl, pGEX	This study	pZS230
EMTB-mCherry	[36]	Addgene 26742
Software and Algorithms		
Fiji version 2.1.0/1.53c	[37]	RRID:SCR_002285
MATLAB version 2016b	MathWorks	RRID:SCR_001622
Prism version 8.3.0 (328)	GraphPad	RRID:SCR_002798

RESOURCE AVAILABILITY

Lead contact

Requests for resources and reagents should be directed to and will be fulfilled by the Lead Contact, Iain Cheeseman (icheese@wi.mit.edu).

Materials availability

Plasmids generated in this study have been deposited with Addgene. All unique/stable reagents generated in this study are available from the Lead Contact with a completed Materials Transfer Agreement.

Data and code availability

- Original western blot images and image quantification values have been deposited with Mendeley Data and are publicly available as of the date of publication (DOI listed in the Key Resources Table). All other data, including microscopy data, are available from the Lead Contact on request.
- This paper does not report original code.
- Any additional information required to reanalyze the data reported in this paper is available from the Lead Contact upon request.

EXPERIMENTAL MODEL AND SUBJECT DETAILS

Sea stars *(Patiria miniata)* were wild-caught by South Coast Bio Marine, kept in artificial seawater aquariums at 15°C, and fed *ad libitum* with frozen shrimp. As they were wild collected animals, genetic backgrounds are mixed and ages are undefined. Individuals were randomly selected for isolation of oocytes or sperm. Males and females were housed in separate aquaria to avoid spawning. Intact ovary and testis fragments were surgically extracted from small incisions on the oral side of the animal using forceps and kept in filtered seawater containing 10 μg/mL trimethoprim and 50- μg/mL sulfamethoxazole at 15°C.[38] The ovary fragments were transferred to fresh seawater and antibiotics every 2 days, and oocytes that were spontaneously released from the ovary were discarded. Intact ovary fragments were cultured this way for up to 1 week until oocytes were to be microinjected for experimentation.

METHOD DETAILS

Oocyte Culture

Isolated oocytes were cultured for a maximum of 24 h in artificial seawater with 10 μg/mL trimethoprim and 50 μg/mL sulfamethoxazole. To induce meiotic resumption, 1-methyladenine (Acros Organics) was added to the culture at a final concentration of 10 mM.

For fertilization, extracted sperm was added to the culture at a 1:1,000,000 dilution. Latrunculin b was used at a final concentration of 10 mM, and nocodazole was used at 3.3 mM. For knockdown of maternal Fzd1 (e.g., Figures 4D and 4E), oocytes were injected with 500 mM morpholino and cultured for 2 days in sulfamethoxazole/trimethoprim-containing seawater (50 mg/mL sulfamethoxazole, 10 mg/mL trimethoprim).

Construct and antibody generation

Patiria miniata gene homologs were identified using genomics tools at echinobase.org.[39] Fluorescent protein fusion constructs for mRNA *in vitro* transcription were cloned into vectors derived from pCS2+8 using standard restriction enzyme-based methods.[40] *Dvl* protein corresponding to the DIX domain (residues 1-90) was expressed as an n-terminal GST fusion in the pGEX-6P vector in BL21 bacteria. Expression was induced with 0.1 mM IPTG and the cells were grown overnight at 18°C. GST-DIX was then purified from bacterial lysate using Glutathione-agarose (Sigma), eluted with reduced L-glutathione (Sigma). Using this immunogen, antibodies were then generated in rabbits (Covance). For affinity purification, serum was pre-depleted against GST, and then purified with GST-DIX bound to HiTrap NHS-activated columns (GE Healthcare). EMTB-mCherry was a gift from William Bement (Addgene plasmid # 26742 ; http://n2t.net/addgene:26742 ; RRID:Addgene_26742).[36]

Oocyte Microinjection and Manipulation

For expression of constructs in oocytes, plasmids were linearized with NotI to yield linear template DNA. mRNA was transcribed *in vitro* using mMessage mMachine SP6 and the polyadenylation kit (Life Technologies), then precipitated using lithium chloride solution. Prophase I arrested oocytes were injected horizontally in Kiehart chambers with 10-20 picoliters of mRNA solution in nuclease free water as described.[38] Dvl-GFP wildtype and mutant constructs were injected at 800 ng/mL. After microinjection, oocytes were cultured 18-24 h to allow time for the constructs to translate before 1-methyladenine stimulation. Custom synthesized morpholinos, or the Gene Tools standard control, were injected at 1000 mM for Dvl and 500 mM for Fzd1 (Gene Tools). For microsurgery experiments (Figure 4A; Figures S4C and S4D), oocytes were cut by hand using a pulled capillary tube as a knife and a mouth pipette to hold in place. For shape mold experiments (Figures S4A and S4B), chambers were fabricated by casting PDMS onto patterned silicon wafers as described previously.[29] The chamber shapes were designed with a height of 80 μm and surface area of around 27000 μm2, to match typical volumes of the oocytes. The patterned silicon wafer was manufactured using photolithography (Microfactory SAS, France). The silicon wafer was silanized with Trichlorosilane (Sigma 448931). PDMS was made by mixing Dow SYLGARD 184 Silicone Elastomer Clear solution at a 10:1 base-to-curing agent ratio. After mixing thoroughly, the elastomer was poured over the silicon master mold, degassed in a vacuum chamber and cured at 60°C in an oven for one h.

Immunofluorescence, *In Situ* Hybridization, and Imaging

For endogenous Dvl immunofluorescence (Figure 4D; Figures S1C and S1D), oocytes were fixed at various stages in a microtubule stabilization buffer (1% paraformaldehyde, 0.1% Triton X-100, 100 mM HEPES, pH 7.0, 50 mM EGTA, 10 mM $MgSO_4$, 400 mM dextrose) for 15 min at room temperature.[41] The oocytes were then transferred to a solution of 80% methanol, 20% DMSO, and incubated on ice for at least 1 h and up to overnight. Oocytes were then washed 3 times in PBS with 0.1% Triton X-100 (PBSTx), transferred to sodium citrate buffer (10 mM tri-sodium citrate dihydrate, 0.05% Tween 20, pH 6.0) and heated at 55°C for 1 h for antigen retrieval. Oocytes were then washed 3 times with PBSTx and blocked for 15 min in AbDil (3% BSA, 1 X TBS, 0.1% Triton X-100, 0.1% Na Azide). Primary antibodies diluted in AbDil were then applied and the oocytes were incubated overnight at room temperature. Anti-alpha tubulin (DM1a, Sigma) and Dishevelled (this study) antibodies were used at 1:5,000. DNA was stained with Hoechst. GFP fusion construct expressing oocytes were instead fixed with 2% PFA in Millonig's Buffered Fixative (0.2 M NaH_2PO_4*H_2O, 0.136 M NaCl, pH 7.0) overnight at room temperature, permeabilized by three washes with PBSTx, and blocked with AbDil as described above. GFP booster (Chromotek) was used at 1:1000 to improve the signal from GFP fusion constructs (e.g., Figures 4C and 4D; Figures S2A–S2D). The oocytes were compressed under coverslips in ProLong Gold Antifade Mountant (ThermoFisher).

Fluorescent whole mount *in situ* hybridization (FISH) was performed as previously described.[42] Embryos were collected and left in fixation solution (4% paraformaldehyde, 32.5% sea water, 32.5 mM MOPS pH 7, 162.5 mM NaCl) overnight at 4°C, then washed in MOPS and stored in 70% ethanol. After rehydration, embryos were hybridized with the Frzd1 probe (0.1 ng/mL) in hybridization buffer (70% formamide, 100 mM MOPS pH 7, 500 mM NaCl, 0.1%Tween 20, 1 mg/mL BSA.) at 60°C for a week. Signal was developed with the fluorophore-conjugated tyramide kit (Perkin Elmer, Cat. #:NEL752001KT; RRID:AB_2572409). After post hybridization washes in maleic acid buffer, embryos were blocked in the blocking buffer provided by the kit and left overnight with anti-digoxigenin-peroxidase antibody (Roche cat #11207733) diluted 1:2000. Signal was detected by staining for 30 min in 1:400 cy3 in amplification diluent (provided in the kit).

Fixed oocytes were imaged with a Nikon Ti2 microscope with a CoolSnap HQ2 CCD camera and a 100x 1.40 NA Olympus U-PlanApo objective (Figure S2D), or a Zeiss 710 confocal **(**Figure S1-4**)**. Live confocal imaging was performed with a Yokogawa W1 spinning disk microscope (Figures 2, 3**, and** 4**;** Figures S3A, S3E, and S3F) or a Zeiss 710 (Figure S4B). Images were processed with Fiji, and scaled equivalently across conditions unless otherwise specified.[37] For images collected with the Zeiss 710 in Figures 4C and 4D; Figures S1D, S3C,D, S4F; the ROF Denoise plugin in Fiji was used with theta value 5.

RNA extraction and quantitative real-time PCR (qPCR)

RNA from 100 embryos was isolated with the RNeasy Micro kit (QIAGEN, Cat#:74004). RNA was quantified with a nanodrop and the whole pool of embryos was used to make cDNA. cDNA synthesis was performed using Maxima kit (Life Technologies, Cat#:K1641) and random hexamer primers were used to prime synthesis of first strand cDNA. qPCR was performed using ABI900 real time instrument with Maxima SYBR master mix (Life Technologies, Cat#:FERK0222). qPCR volume was 25 mL per well containing 1 mL of cDNA diluted 1:10 (1 embryo equivalent), 2.5 pMoles of each primer (forward and reverse), 12.5 mL of SybrGreen Mix and water. The integrity of the amplicons was determine by melt curves. ddCt values were calculated between experiment and control embryos and converted to fold differences using ubiquitin as a reference (FD = 2 DDCt).Experiments were run in two biological replicates, and each biological replicate was run on the qPCR machine with three technical replicates.

QUANTIFICATION AND STATISTICAL ANALYSIS

Statistical analyses were performed using Prism (8.3.0 GraphPad Software). Details of statistical tests and sample sizes are provided in the figure legends. Unless stated otherwise in the figure legends, images comparing the same signal across conditions are scaled equivalently. In all cases in which pixel intensity is quantified, unscaled images with appropriate background subtraction were used, as outlined below.

Kymograph depictions of Dvl localization dynamics (Figure 1E) were generated in MATLAB. The space time kymograph of cytoplasmic Dvl $I_C(y,t)$ was obtained by extracting the fluorescence intensity $I_C(y)$ along the animal-vegetal (AV) axis for all time frame t. Here, we used y to denote the distance along AV axis. We first performed a Gaussian filtering step (with standard deviation of 2 pixels) to smooth the fluorescence image. We then computed the average of the intensity values 10 pixels to the left and to the right of the AV axis to obtain $I_C(y)$. To construct the full kymograph $I_C(y,t)$, the intensity $I_C(y)$ at each time frame t is aligned such that the animal and vegetal poles correspond to the same position and resampled at the appropriate distance y. The space time kymograph of cortical fluorescence $I_R(s,t)$ is computed by first extracting the boundary of the oocyte $\vec{r}(s) = (x(s), y(s))$ and then extracting the fluorescence intensity $I_R(s)$ along the boundary for all time frames t. Here, we used s to parameterize the arclength of the oocyte boundary. For each time frame t, we performed a Gaussian filtering step (with a standard deviation of 1.2 pixels) before applying a thresholding step to make a binary image. The oocyte boundary $\vec{r}(s)$ is obtained by using the *bwboundaries* function in MATLAB on the binary image. The intensity $I_R(s)$ is obtained by first identifying a local window of size 8-by-8 pixels centered at $\vec{r}(s)$ and taking the mean intensity of the pixels in the top 50 percentile intensity within the local window. To construct the full kymograph $I_R(s,t)$, the intensity $I_R(s)$ at each time frame t is aligned such that the AP corresponds to the same arclength position and resampled at the appropriate arclength s.

To segment the cortical and cytoplasmic Dvl puncta at a single time point (Figures 2B–2D), each z slice of the confocal z stack was first demarcated into a cytoplasmic and a cortical region. By applying a thresholding to identify the boundary of the oocyte, the region around 30 pixels (3.25 μm) extending from the cell boundary into the cytoplasm is defined as the cortical region, while the rest of the oocyte is considered the cytoplasmic region. After performing this step on all z-slices, a maximum intensity projection is done separately on the cortical and cytoplasmic region. To segment the Dvl puncta in the respective region, a 2D Gaussian blur is first performed before a thresholding step. Once the binary image is obtained, the MATLAB function *regionprops* is used to calculate the area and centroid of each puncta. The mean squared displacement with respect to initial position is calculated as $MSD(t) = (\vec{r}(t) - \vec{r}(t = 0))$, where the average is done over all available puncta. To generate the plot of mean velocity as a function of angle, the instantaneous velocity along the puncta trajectory is first calculated as $\vec{v}(t) = (\vec{r}(t + dt) - \vec{r}(t))/dt$, where dt is the frame duration. All recorded instantaneous velocities were then binned according to the angle they make with the x-axis.

To quantify the fraction of Dvl co-localizing with Lamp1+ endosomes (Figure 3E; Figure S3F), the segmentation of Dvl puncta and Lamp puncta were first performed separately. Briefly, a 2D Gaussian blur was performed before the appropriate thresholding step was applied to obtain a binary image for each channel. The fraction of Dvl on endosome f_{Dvl} is calculated as $f_{Dvl} = A_{Dvl \cap Lamp} / A_{Dvl}$, where $A_{Dvl \cap Lamp}$ is the total area of all Dvl puncta that overlap with Lamp puncta, and A_{Dvl} is the total area of all Dvl puncta. The final reported f_{Dvl} is the temporal mean averaged over the appropriate cell cycle duration.

Quantification of cortex-associated Dvl signal was performed using Fiji.[37] To measure the pixel intensity of Dvl localized to the membrane in Figure 4F, a single z-slice encompassing the membrane was selected. A 50-pixel circular region of interest was defined within the vegetal Dvl domain, and a background area was defined in an in-focus region of the oocyte membrane but outside of the Dvl domain. These regions were measured using *RawIntDen* parameter, and the background was subtracted from the Dvl measurement. These background subtracted values were then normalized to the mean of the control oocytes. For quantification of Dvl mutants (Figures S3E and S3F) background subtraction was performed using a rolling ball radius of 1 pixel and the sliding paraboloid function. *Gaussian Blur* was then applied with radius of 1 pixel. Next, *Auto Threshold* was performed using the *Triangle* method. To identify puncta, the *Watershed* function followed by *Analyze Particles* was performed to create a selection of ROIs that were then applied to the original image, and then the intensities were determined with *Measure* and the *RawIntDen* parameter. The total number of puncta are reported relative to image area in square microns, along with the mean of *RawIntDen* across puncta per individual oocyte.